

# 光学学报

## 高衍射效率低偏振灵敏度全反射浸没光栅的设计

陈慧盈<sup>1,2,3</sup>, 陈新华<sup>1,2,3\*</sup>, 潘俏<sup>1,2,3</sup>, 朱嘉诚<sup>1,2,3</sup>, 沈为民<sup>1,2,3</sup>

<sup>1</sup>苏州大学光电科学与工程学院, 江苏苏州 215006;

<sup>2</sup>江苏省先进光学制造技术重点实验室, 江苏苏州 215006;

<sup>3</sup>教育部现代光学技术重点实验室, 江苏苏州 215006

**摘要** 浸没光栅是星载温室气体监测成像光谱仪光学系统中的核心分光元件, 能够实现更高的光谱分辨率和更紧凑的结构尺寸。推导了浸没光栅的色散率公式, 并对比了采用浸没光栅和普通平面光栅时的光谱分辨率。针对温室气体 O<sub>2</sub>-A 带的探测需求, 利用有限元计算方法开展了浸没光栅槽形结构的优化设计, 得到了兼有高衍射效率和低偏振灵敏度的全反射型浸没光栅槽形参数, 并分析了光栅结构参数和等效介质层的制造公差。设计结果表明, 在 750~770 nm 波段范围内, 该浸没光栅一级平均衍射效率高于 92%, 偏振灵敏度低于 1%。

**关键词** 衍射光栅; 浸没光栅; 全反射; 等效介质层; 衍射效率; 偏振灵敏度

中图分类号 TH744

文献标志码 A

DOI: 10.3788/AOS231040

### 1 引言

由于人类活动引起的化石燃料燃烧、森林植被破坏以及工业生产排放等, 地球大气中温室气体浓度逐年增加<sup>[1]</sup>。根据世界气象组织发布的报告, 全球二氧化碳浓度于 2020 年达到  $413.2 \times 10^{-6}$ , 是有史以来观测到的最高值。二氧化碳的持续排放会导致全球温度上升, 引起高温、强降雨和海平面上升等天气极端事件, 从而产生深远的社会经济影响。对温室气体进行科学、准确的监测是了解和掌握温室气体排放情况, 了解地球气候演变规律的重要保障。与其他观测手段相比, 通过卫星观测温室气体浓度具有覆盖面积大、响应快速以及可实现长期监测等优势, 是国内外获取温室气体数据的重要手段之一。

光栅型成像光谱仪具有高分辨本领、高信噪比以及色散接近线性等优点, 是星载温室气体监测的重要光学载荷之一<sup>[2]</sup>。随着提高光谱分辨率和减小仪器体积等需求的提出, 浸没光栅逐渐被用于星载温室气体监测成像光谱仪中。与传统光栅相比, 浸没光栅在同等尺寸下具有更高的光谱分辨本领<sup>[3]</sup>。

硅浸没光栅和石英浸没光栅是星载温室气体监测成像光谱仪中常见的两类浸没光栅。2012 年, 英国 SSTL 公司研制了工作在近红外(NIR)通道的石英浸没光栅, 光栅槽密度为 3226 lp/mm。测试结果表明,

该光栅的平均效率超过 70%, 偏振灵敏度低于 10%<sup>[4]</sup>。2012 年, 欧洲航天局提出的 CarbonSat 方案中采用了硅浸没衍射光栅<sup>[5]</sup>。2017 年, 欧洲 Sentinel-5P 卫星搭载的对流层监测仪器(TROPOMI)中使用了硅浸没衍射光栅, 光栅槽密度为 400 lp/mm, 平均衍射效率大于 60%, 偏振灵敏度小于 10%<sup>[6]</sup>。计划于 2024 年发射的 Sentinel-5 卫星中采用了硅浸没衍射光栅, 其中, SWIR-1 通道的光栅衍射效率大于 59%, 偏振灵敏度小于 13%, SWIR-3 通道的光栅衍射效率大于 55%, 偏振灵敏度小于 17%<sup>[7]</sup>。计划于 2025 年发射的 Sentinel-7 卫星中采用了石英浸没光栅, 在 SWIR-1 工作波段内光栅的平均效率超过 90%, 偏振灵敏度低于 10%<sup>[8]</sup>。在国内, 苏州大学于 2020 年研制了基于石英浸没光栅的温室气体监测仪光学系统, 该系统在 752.5~767.5 nm 波段下的光栅平均衍射效率设计值大于 85%, 偏振灵敏度设计值约 5%<sup>[9]</sup>。

针对温室气体光谱探测的应用需求, 本文提出并设计了一种工作在全反射条件下的反射式石英浸没光栅, 光栅衍射效率大于 92%, 偏振灵敏度小于 1%。该光栅具有以下两个主要特点: 1) 光栅面的光束入射角大于石英的全反射角, 光栅无透射级次, 光能量集中在反射衍射级上, 有利于光栅衍射效率的提高<sup>[10]</sup>; 2) 光栅表面镀有均匀高折射率介质层, 能够提高光栅在 TE 和 TM 方向的衍射效率, 降低光栅的偏振灵敏度<sup>[11]</sup>。

收稿日期: 2023-05-24; 修回日期: 2023-06-30; 录用日期: 2023-07-25; 网络首发日期: 2023-08-02

基金项目: 国家自然科学基金(62105230)、江苏高校优势学科建设工程(PAPD)、苏州市产业前瞻与关键核心技术项目(SYC2022142)

通信作者: \*xinhua\_chen@suda.edu.cn

本文首先介绍浸没光栅的原理及槽形结构,然后根据光学设计给出的光栅参数及使用条件,设计并优化光栅槽形参数,并对等效介质层进行设计,最后对所设计的光栅进行了制造公差的分析。

## 2 工作原理及槽形结构

与普通光栅不同,浸没光栅的光栅面制作在材料基底的后表面,如图 1 所示。图中棱镜基底的折射率为  $n$ ,顶角为  $A$ 。入射光以角度  $i_1$  从面  $S_1$  入射,其折射角为  $i_2$ ; 折射光在光栅面  $G$  上的入射角为  $\alpha$ ,其反射级别的衍射角为  $\beta$ ; 衍射光入射到面  $S_1$  上的入射角为  $i_3$ ,在面  $S_1$  上的折射角为  $i_4$ 。

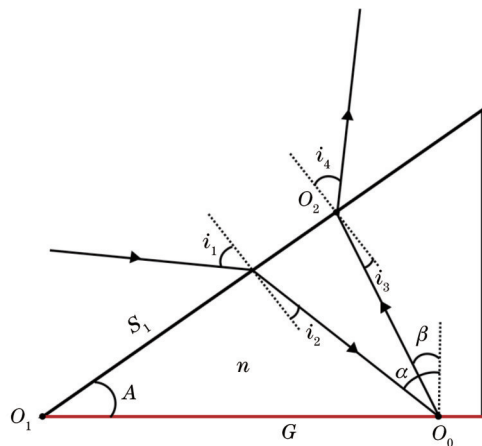


图 1 浸没光栅原理图

Fig. 1 Schematic diagram of immersed grating

由光栅方程可得

$$nd(\sin \alpha + \sin \beta) = m\lambda, \quad (1)$$

式中: $n$  为棱镜折射率; $d$  为光栅周期; $m$  为衍射级次; $\lambda$  为光波长。

由折射定律可知

$$\sin i_1 = n \sin i_2, \quad (2)$$

$$n \sin i_3 = \sin i_4. \quad (3)$$

联立式(1)、(3),可得浸没光栅的角色散率为

$$\frac{di_4}{d\lambda} = \frac{n \cos i_3}{\cos i_4} \cdot \frac{(\sin \alpha + \sin \beta)}{\lambda \cos \beta}. \quad (4)$$

假设用于接收浸没光栅出射光的聚焦镜头焦距为  $f$ ,则可知光栅线色散率为

$$\frac{dl}{d\lambda} = f \cdot \frac{di_4}{d\lambda} = f \cdot \frac{n \cos i_3}{\cos i_4} \cdot \frac{(\sin \alpha + \sin \beta)}{\lambda \cos \beta}. \quad (5)$$

由此可得,当  $\alpha$ 、 $\beta$  和  $\lambda$  相同时,浸没光栅的角色散率和线色散率是普通平面光栅的  $\frac{n \cos i_3}{\cos i_4}$  倍。采用具有高折射率的棱镜材料,能够有效提高光栅的角色散率和线色散率。

假设光谱仪器狭缝的单色像宽度为  $\Delta x'$ ,可得光谱仪光谱分辨率  $\Delta\lambda^{[12]}$  为

$$\Delta\lambda = \frac{\Delta x'}{\frac{dl}{d\lambda}} = \frac{\Delta x'}{f \cdot \frac{di_4}{d\lambda}}. \quad (6)$$

由式(6)可知,相较于普通平面光栅,使用浸没光栅时的光谱分辨率提高了  $\frac{n \cos i_3}{\cos i_4}$  倍。由此可得,在相同的光谱分辨率要求下,使用浸没光栅可使光学系统焦距缩小  $\frac{n \cos i_3}{\cos i_4}$  倍,相应光学系统体积能够缩小约  $\left(\frac{n \cos i_3}{\cos i_4}\right)^3$  倍。

当光栅入射角  $\alpha$  大于棱镜基底材料的全反射角  $\theta_{\text{TIR}}$  时,浸没光栅可称为全反射浸没光栅。全反射浸没光栅角色散率、线色散率和光谱分辨率与普通浸没光栅一致,但无透射衍射级次,仅存在反射衍射级次光,有利于光栅衍射效率的提高。

虽然光栅工作在全反射条件下,但由于倏逝波的存在,通常会在光栅表面镀制金属反射膜,增加光栅的衍射效率<sup>[13]</sup>。考虑到等离子体效应产生的共振吸收,金属反射膜的存在可能导致光栅的偏振灵敏度升高<sup>[14]</sup>;同时,金属膜层难以实现保型镀膜,膜层和光栅槽形间的空隙会导致光栅效率下降。为了进一步提高光栅的衍射效率,并降低光栅的偏振灵敏度,可在光栅槽形结构上均匀覆盖一层高折射率的氧化物介质层<sup>[11,15-16]</sup>。此时,光栅的槽形结构示意图如图 2 所示,等效介质层均匀地覆盖在矩形光栅槽形结构上,其横向和纵向的厚度是一致的。图中, $h$  是光栅槽深, $L$  是等效介质层厚度, $d$  是光栅周期。光栅占空比  $\tau$  定义为  $b$  与  $d$  的比值,深周期比  $\rho$  定义为  $h$  与  $d$  的比值。下文将基于此槽形结构开展光栅设计。

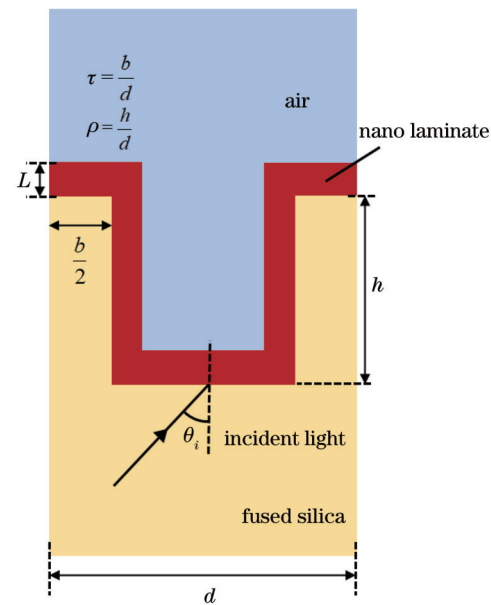


图 2 光栅槽形结构示意图

Fig. 2 Schematic diagram of grating groove structure

### 3 结构参数设计

本文研制的全反射浸没光栅用于温室气体监测载荷的O<sub>2</sub>-A带探测通道,根据光学系统设计给出的输入,光栅主要光学参数如表1所示。由光栅周期可知,光栅仅有-1级和0级衍射。光栅入射角为71.4°,大于全反射角(熔融石英材料 $\theta_{\text{TIR}}=44^\circ$ )。

表1 浸没光栅主要光学参数

Table 1 Main optical parameters of immersed grating

Parameter	Value
Wavelength /nm	750~770
Groove density /(lp·mm <sup>-1</sup> )	3550
Diffraction order	-1
Incidence angle /(°)	71.4
Substrate material	Fused silica

根据前期工作,光栅的初始结构参数取值如表2所示。利用COMSOL软件进行建模仿真,得到的衍射效率以及偏振灵敏度曲线如图3所示。

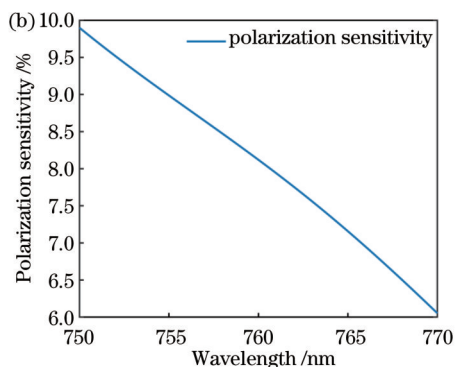
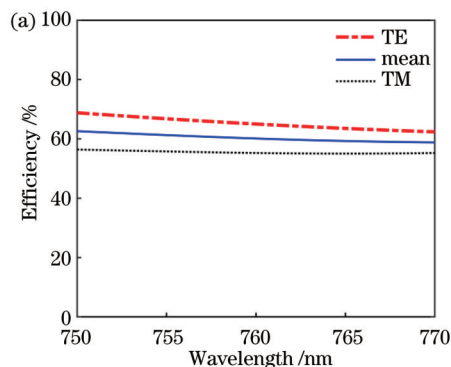


图3 光栅初始结构衍射效率及偏振灵敏度曲线。(a)衍射效率;(b)偏振灵敏度

Fig. 3 Grating initial structure diffraction efficiency and polarization sensitivity curve. (a) Diffraction efficiency; (b) polarization sensitivity

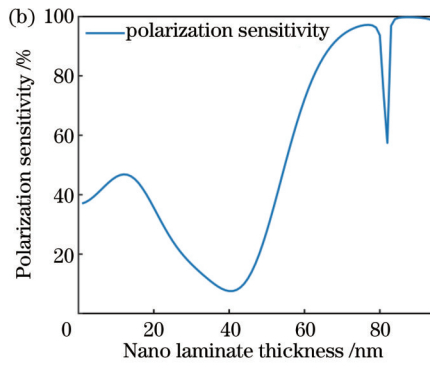
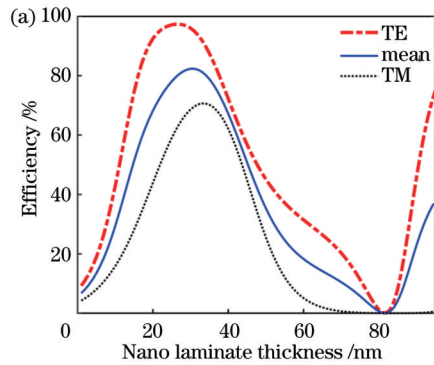


图4 不同等效介质层厚度下的衍射效率及偏振灵敏度。(a)衍射效率;(b)偏振灵敏度

Fig. 4 Diffraction efficiency and polarization sensitivity at different nano laminate thicknesses. (a) Diffraction efficiency; (b) polarization sensitivity

2)确定光栅占空比。保持光栅槽深和等效介质层折射率不变,计算不同等效介质层厚度和占空比时中心波长处的衍射效率和偏振灵敏度。等效介质层的厚

度取值范围为17~48 nm,光栅占空比取值范围为0.12~0.86。根据计算结果,得到平均衍射效率高于90%且偏振灵敏度低于1%时对应的等效介质层厚度

表2 光栅初始结构参数

Table 2 Grating initial structure parameters

Parameter	Value
Duty cycle	0.3
Groove depth /nm	250
Nano laminate thickness /nm	43
Refractive index of nano laminate $n$	2

接下来以光栅初始结构为基础,优化光栅结构参数,进一步提高光衍射效率,并降低光栅偏振灵敏度,具体步骤如下。

1)确定等效介质层的厚度范围。使用控制变量法,固定浸没光栅槽深、占空比和等效介质层折射率,使等效介质层厚度从1 nm变化到95 nm,得到中心波段下衍射效率和偏振灵敏度的变化曲线,如图4所示。根据中心波段下平均衍射效率大于60%且偏振灵敏度低于20%对应的厚度范围,等效介质层的厚度范围确定为17~48 nm。

和光栅占空比,如表3所示。由此得到,随着占空比的增加,平均衍射效率下降,偏振灵敏度变化不大。根据表中数据,最终取光栅占空比为0.14,等效介质层厚度为42 nm。

表3 筛选后得到的不同占空比和等效介质层厚度下的衍射效率和偏振灵敏度

Table 3 Diffraction efficiency and polarization sensitivity under different duty cycles and nano laminate thicknesses after screening

Duty cycle	Nano laminate thickness / nm	Average efficiency / %	Polarization sensitivty / %
0.12	43	98.73	0.11
0.14	42	98.25	0
0.16	42	97.14	0.25
0.18	41	95.96	0.20
0.20	41	93.65	0.20
0.22	41	90.35	0.40

### 3)确定光栅槽深。

选取光栅占空比和等效介质层厚度后,需要确定

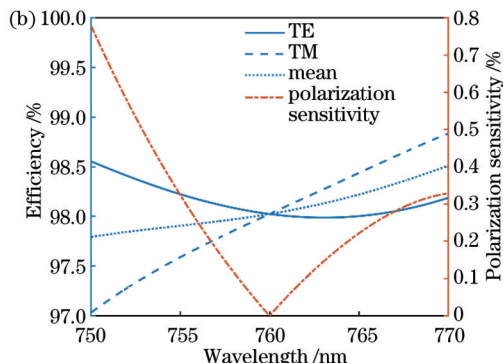
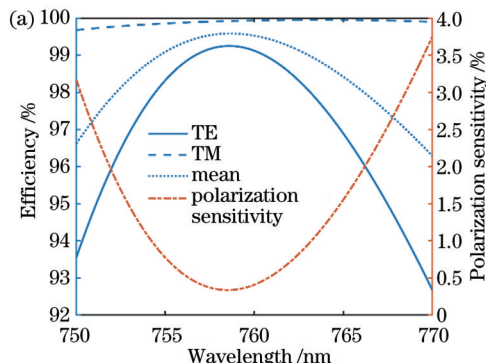


图5 光栅槽深为248 nm时不同等效介质层折射率下的衍射效率及偏振灵敏度。(a)折射率为2.3;(b)折射率为2

Fig. 5 Diffraction efficiency and polarization sensitivity at different refractive indices of nano laminate for the grating groove depth of 248 nm. (a) Refractive index is 2.3; (b) refractive index is 2

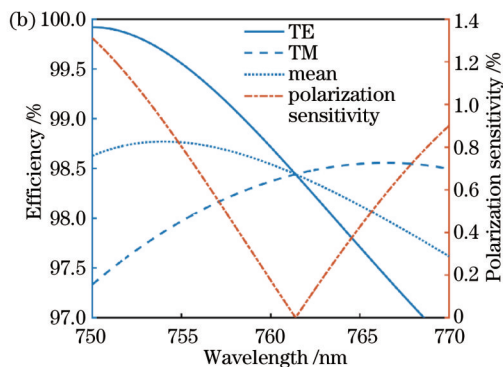
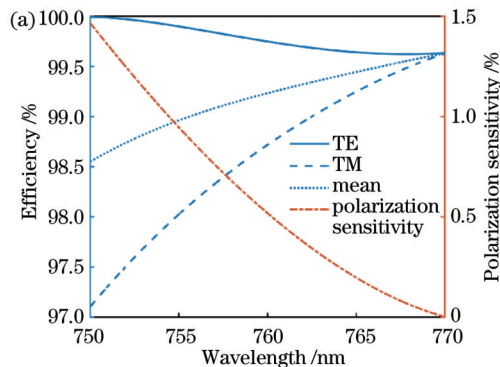


图6 光栅槽深为268 nm时不同等效介质层折射率下的衍射效率及偏振灵敏度。(a)折射率为2;(b)折射率为2.1

Fig. 6 Diffraction efficiency and polarization sensitivity at different refractive indices of nano laminate for the grating groove depth of 268 nm. (a) Refractive index is 2; (b) refractive index is 2.1

根据图5和图6中的曲线可知,最佳衍射效率与偏振灵敏度曲线如图5(b)所示,光栅在该参数下偏振灵

敏度既能小于1%,平均衍射效率又能大于97.5%,可以达到高衍射效率低偏振灵敏度的效果,因此光栅最

4)确定等效介质层折射率。在以上参数确定后,继续确定能使光栅获得更佳性能的等效介质层折射率。固定浸没光栅的占空比、槽深和等效介质层厚度,只改变等效介质层折射率,使其变化范围为1.5~3。在两个不同的光栅槽深(248 nm和268 nm)下,分别计算光栅中心波段下的衍射效率和偏振灵敏度。通过数据分析:当光栅槽深为248 nm时,最高平均衍射效率对应的等效介质层折射率为2.3,最低偏振灵敏度对应的等效介质层折射率为2;当光栅槽深为268 nm时,最高平均衍射效率对应的等效介质层折射率为2,最低偏振灵敏度对应的等效介质层折射率为2.1。

图5是槽深为248 nm、光栅占空比为0.14、等效介质层厚度为42 nm时,等效介质层折射率分别为2.3和2的衍射效率和偏振灵敏度曲线。图6是槽深为268 nm,占空比和等效介质层厚度与图5相同时,介质层折射率分别为2和2.1的光栅衍射效率及偏振灵敏度曲线。

优结构参数如表4所示。

表4 优化后的浸没光栅结构参数

Table 4 Optimized immersed grating structure parameters

Parameter	Value
Wavelength /nm	750~770
Groove density /(lp·mm <sup>-1</sup> )	3550
Diffraction order	-1
Incidence angle /(°)	71.4
Duty cycle	0.14
Groove depth /nm	248
Nano laminate thickness/nm	42
Refractive index of nano laminate $n$	2
Substrate material	Fused silica

#### 4 等效介质层膜系设计

本文设计的浸没光栅采用了等效介质层,还需要不同材料、不同厚度的材料叠加,使得该层的折射率为2,且不影响光栅衍射效率和偏振灵敏度。等效介质层的膜系设计可采用薄膜光学的设计方法,先选择构成多层膜的膜系材料<sup>[17]</sup>。

表5 等效介质层多层膜叠加设计结果

Table 5 Nano laminate design results

Parameter	Value
Number of layers of film system	5
Film system structure	Al <sub>2</sub> O <sub>3</sub> -TiO <sub>2</sub> -Al <sub>2</sub> O <sub>3</sub> -TiO <sub>2</sub> -Al <sub>2</sub> O <sub>3</sub>
Nano laminate total thickness /nm	55
Refractive index of nano laminate $n$	2
Thickness of each layer of film /nm	11-11-11-11-11

将上述设计结果进行计算,得到所设计光栅的衍射效率与偏振灵敏度曲线,如图8所示。最终光栅的

本文选择常见的Al<sub>2</sub>O<sub>3</sub>(折射率为1.67)和TiO<sub>2</sub>(折射率为2.10)两种材料交替叠加,形成的多层膜具有非常低的光学损耗(指散射和吸收损耗)<sup>[18-19]</sup>。根据薄膜光学设计原理,结合实际加工难度,优化纳米层的厚度和叠加顺序,最后优化得到的等效介质层多层膜叠加结构如图7所示,优化结果如表5所示。

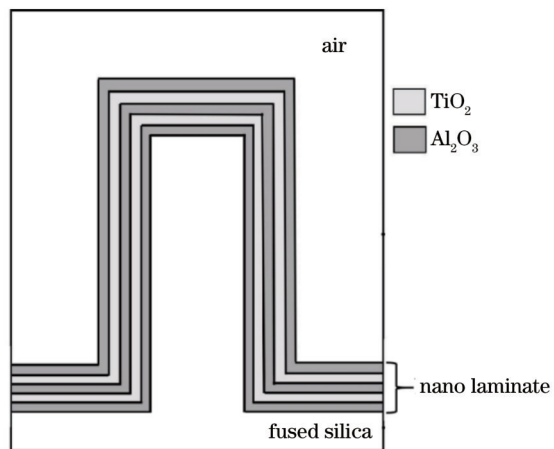


图7 等效介质层多层膜叠加结构

Fig. 7 Nano laminate structure

设计结果为工作波段内衍射效率大于92%,偏振灵敏度小于1%。

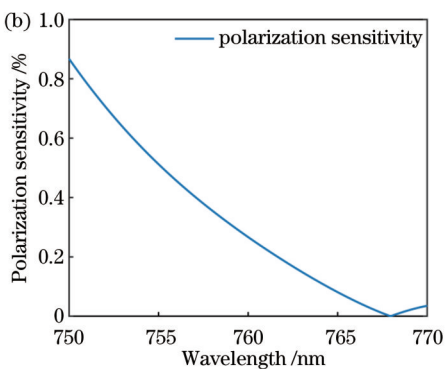
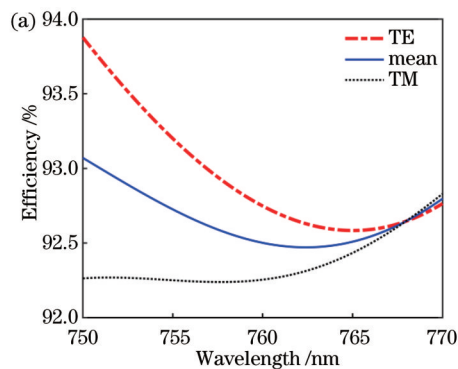


图8 五层介质膜叠加后光栅的衍射效率及偏振灵敏度。(a)衍射效率;(b)偏振灵敏度

Fig. 8 Diffraction efficiency and polarization sensitivity of grating after five-layer film stacking. (a) Diffraction efficiency; (b) polarization sensitivity

#### 5 制造公差分析

在光栅制造过程中,常见的加工误差主要有深周

期比误差、占空比误差以及等效介质层厚度误差等,这些误差会影响光栅性能,导致衍射效率下降或偏振灵敏度的上升,因此需要分析并制定合理的公差值。

图 9 和图 10 分别为光栅深周期比与占空比同时变化时, 中心波长处平均衍射效率及偏振灵敏度的数值分布图, 其中深周期比的取值范围为 0.4~2, 占空比取值范围为 0.12~0.7。

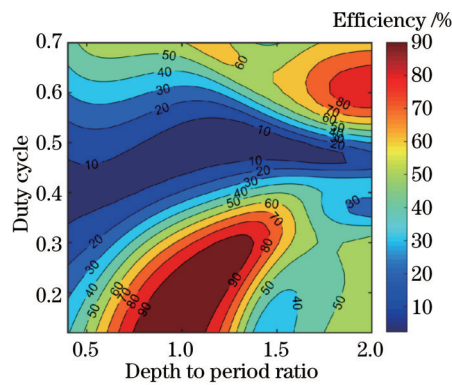


图 9 不同深周期比与占空比下的平均衍射效率

Fig. 9 Average diffraction efficiency at different depth to period ratios and duty cycles

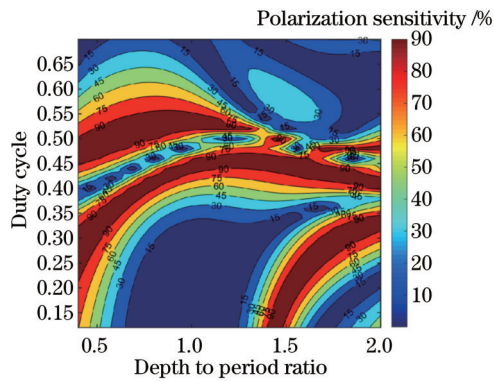


图 10 不同深周期比与占空比下的偏振灵敏度

Fig. 10 Polarization sensitivity at different depth to period ratios and duty cycles

取最高平均衍射效率的下降不大于 10% 为筛选依据, 得到占空比和深周期比的变化范围如图 11 所示。图中的点代表满足要求的占空比和深周期比, 最

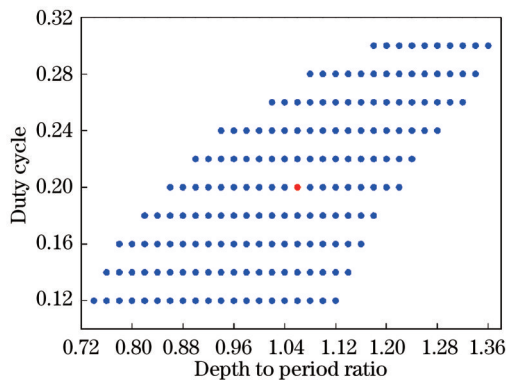


图 11 衍射效率下降小于 10% 时深周期比与占空比的制造公差  
Fig. 11 Tolerance of depth to period ratio and duty cycle when diffraction efficiency decreases is less than 10%

高平均衍射效率对应的占空比为 0.2, 深周期比为 1.06。

取平均偏振灵敏度不大于 1% 为筛选依据, 得到如图 12 所示的制造公差。每个点代表对应的占空比和深周期比。最低平均偏振灵敏度对应的占空比为 0.16, 深周期比为 0.86。

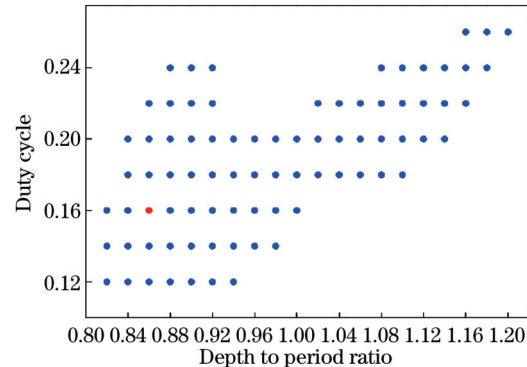


图 12 偏振灵敏度小于 1% 时深周期比与占空比的制造公差

Fig. 12 Tolerances of depth to period ratio and duty cycle when polarization sensitivity is less than 1%

将图 11 和图 12 结合得到本文设计的全反射浸没光栅的槽形结构制造公差, 如图 13 所示。

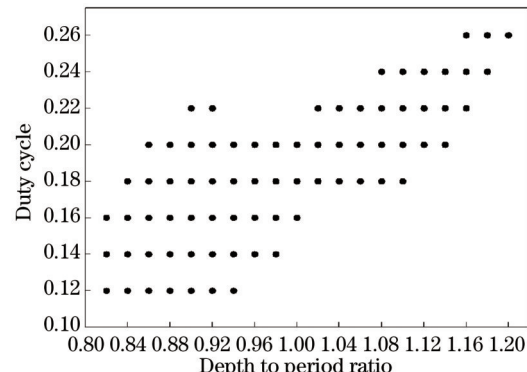


图 13 光栅的深周期比与占空比公差

Fig. 13 Tolerance of depth to period ratio and duty cycle tolerances of the grating

同时, 利用相同分析方法可以分析得到等效介质层中  $\text{Al}_2\text{O}_3$  和  $\text{TiO}_2$  的厚度公差。综上分析, 在满足衍射效率大于 90%、偏振灵敏度小于 1% 的条件下, 光栅深周期比、占空比以及等效介质层叠加材料总厚度的公差范围如表 6 所示。

表 6 浸没光栅制造公差  
Table 6 Manufacturing tolerances of immersed grating

Parameter	Value
Tolerances of duty cycle	-0.08~+0.32
Tolerances of depth to period ratio	-0.02~+0.12
Tolerance of $\text{Al}_2\text{O}_3/\text{nm}$	-6
Tolerance of $\text{TiO}_2/\text{nm}$	+6

## 6 结 论

本文从浸没光栅的原理出发,推导了浸没光栅光谱分辨率公式,表明浸没光栅能够在实现高光谱分辨率的同时减小光学系统的体积。根据光学设计给出的工作条件和光栅参数,选择熔融石英作为光栅基底,优化设计了适用于O<sub>2</sub>-A探测波段的高衍射效率、低偏振灵敏度的全反射浸没衍射光栅。所设计的光栅在工作波段内衍射效率大于92%,偏振灵敏度优于1%。根据光栅衍射效率和偏振灵敏度的要求,分析了相应的制造公差。本文设计的反射式浸没光栅具有高衍射效率和低偏振的优点,槽形公差在制造上具有可行性,相关工作为反射式浸没光栅的设计积累了工作基础。

## 参 考 文 献

- [1] Cubasch U, Wuebbles D, Chen D, et al. Climate change 2013: the physical science basis: contribution of working group I to the fifth assessment report of the intergovernmental panel on climate change[J]. Computational Geometry, 2013, 18(2): 95-123.
- [2] 宋文宝, 靳阳明, 赵知诚, 等. 大气CO<sub>2</sub>甚高光谱分辨率成像光谱仪分析与光学设计[J]. 光学学报, 2015, 35(7): 0722001.  
Song W B, Jin Y M, Zhao Z C, et al. Analysis and optical design of very high spectral resolution imaging spectrometer of the atmospheric CO<sub>2</sub>[J]. Acta Optica Sinica, 2015, 35(7): 0722001.
- [3] Leitner A. The life and work of Joseph Fraunhofer (1787 – 1826) [J]. American Journal of Physics, 1975, 43(1): 59-68.
- [4] Fernandez-Saldivar J, Culfa F, Angli N, et al. Efficiency, dispersion and straylight performance tests of immersed gratings for high resolution spectroscopy in the near infrared[J]. Proceedings of SPIE, 2017, 10564: 105642S.
- [5] Sierk B, Löscher A, Caron J, et al. CarbonSat instrument pre-developments: towards monitoring carbon dioxide and methane concentrations from space[J]. Proceedings of SPIE, 2017, 10562: 105622C.
- [6] van Amerongen A H, Visser H, Vink R J P, et al. Development of immersed diffraction grating for the TROPOMI-SWIR spectrometer[J]. Proceedings of SPIE, 2010, 7826: 78261D.
- [7] Kohlhaas R, Tol P, Schuurhof R, et al. Manufacturing and optical performance of silicon immersed gratings for Sentinel-5 [J]. Proceedings of SPIE, 2019, 11180: 111801L.
- [8] Sierk B, Fernandez V, Bézy J L, et al. The Copernicus CO2M mission for monitoring anthropogenic carbon dioxide emissions from space[J]. Proceedings of SPIE, 2021, 11852: 118523M.
- [9] Pan Q, Shen W M. Optical system of high-precision greenhouse gas imaging spectrometer[J]. Proceedings of SPIE, 2018, 10781: 107810D.
- [10] Marcianò J R, Raguin D H. High-efficiency, high-dispersion diffraction gratings based on total internal reflection[J]. Optics Letters, 2004, 29(6): 542-544.
- [11] Heusinger M, Flügel-Paul T, Grabowski K, et al. High-dispersion TIR-GRISMs with flattened angular dispersion profile [J]. Optica, 2022, 9(4): 412-418.
- [12] 杨子江, 潘俏, 朱嘉诚, 等. 紫外光刻-湿法刻蚀硅中阶梯光栅的研制[J]. 光学学报, 2023, 43(13): 1305001.  
Yang Z J, Pan Q, Zhu J C, et al. Fabrication of silicon echelle grating by ultraviolet lithography combined with wet etching[J]. Acta Optica Sinica, 2023, 43(13): 1305001.
- [13] Ma J Y, Liu T G, Jiang J F, et al. Progress in sensitivity enhancement for optical fibre surface plasmon resonance sensing [J]. Chinese Journal of Lasers, 2021, 48(19): 1906002.  
Ma J Y, Liu T G, Jiang J F, et al. Progress in sensitivity enhancement for optical fibre surface plasmon resonance sensing [J]. Chinese Journal of Lasers, 2021, 48(19): 1906002.
- [14] 王双双, 黄勇林, 詹平. 基于正十六边形光子晶体光纤的表面等离子体共振传感器[J]. 激光与光电子学进展, 2022, 59(7): 0706001.  
Wang S S, Huang Y L, Zhan P. Surface plasmon resonance sensor based on photonic crystal fiber in regular hexadecagon[J]. Laser & Optoelectronics Progress, 2022, 59(7): 0706001.
- [15] Zeitner U D, Fuchs F, Kley E B, et al. High-refractive-index gratings for spectroscopic and laser applications[J]. Proceedings of SPIE, 2014, 8995: 899504.
- [16] 张东阳, 赵磊, 王向贤, 等. 一种基于介质光栅金属薄膜复合结构的折射率传感器[J]. 光学学报, 2017, 37(11): 1124001.  
Zhang D Y, Zhao L, Wang X X, et al. A refractive index sensor based on composite structure of dielectric grating with metal films [J]. Acta Optica Sinica, 2017, 37(11): 1124001.
- [17] Flügel-Paul T, Kalkowski G, Benkenstein T, et al. New grating concepts in the NIR and SWIR spectral band for high resolution earth-observation spectrometers[J]. Proceedings of SPIE, 2016, 9912: 99122A.
- [18] Ratzsch S, Kley E B, Tünnermann A, et al. Influence of the oxygen plasma parameters on the atomic layer deposition of titanium dioxide[J]. Nanotechnology, 2015, 26(2): 024003.
- [19] Ratzsch S, Kley E B, Tünnermann A, et al. Encapsulation process for diffraction gratings[J]. Optics Express, 2015, 23(14): 17955-17965.

## Design of Total Internal Reflection Immersed Gratings with High Diffraction Efficiency and Low Polarization Sensitivity

Chen Huiying<sup>1,2,3</sup>, Chen Xinhua<sup>1,2,3\*</sup>, Pan Qiao<sup>1,2,3</sup>, Zhu Jiacheng<sup>1,2,3</sup>, Shen Weimin<sup>1,2,3</sup>

<sup>1</sup>School of Optoelectronic Science and Engineering, Soochow University, Suzhou 215006, Jiangsu, China;

<sup>2</sup>Key Lab of Advanced Optical Manufacturing Technologies of Jiangsu Province, Suzhou 215006, Jiangsu, China;

<sup>3</sup>Key Lab of Modern Optical Technologies of Education Ministry of China, Suzhou 215006, Jiangsu, China

## Abstract

**Objective** The concentration of greenhouse gases in the earth's atmosphere is increasing year by year under the influence

of fuel burning, deforestation, and industrial development. The continuous emission of greenhouse gases will result in increased global temperature and extreme weather such as heavy rainfall and sea level rise. Remote sensing of greenhouse gases is an important method for tracking greenhouse gas emissions and understanding the earth's climate evolution. As one of the most important optical payloads for spaceborne greenhouse gas monitoring, the grating imaging spectrometer features high resolution, high signal-to-noise ratio, and nearly linear dispersion. The immersed grating can achieve higher spectral resolution and more compact structural size and has been employed as the dispersion elements in imaging spectrometer for remote sensing of greenhouse gases. Currently, immersed gratings with higher performance are required to fulfill the requirements for more accurate greenhouse gas monitoring. For conventional reflective immersed gratings, metallic coatings are adopted to reflect the incident light. However, there are many disadvantages for the metallic coating. Firstly, this coating may cause resonance absorption due to the plasmon effect. The resonance absorption will decrease the diffraction efficiency and increase the polarization sensitivity of the grating. Secondly, it is difficult to deposit metal materials on the grating groove, which will also cause decreased diffraction efficiency. To this end, we propose and design a total internal reflection immersed grating whose grating groove is coated with nano laminate. It has high diffraction efficiency and low polarization sensitivity and can be utilized in the O<sub>2</sub>-A channel for the imaging spectrometer of greenhouse gas monitoring.

**Methods** According to the monitoring requirements of greenhouse gases, the design of the immersed grating is as follows. Firstly, the grating structure is modeled by the finite element software, and the diffraction efficiency and polarization sensitivity of the initial structure are calculated. Then, the parameters such as the duty cycle of the grating, the thickness of the nano laminate, the groove depth, and the refractive index of the nano laminate are optimized in turn with the controlled variable method. According to the optical film theory and the actual coating method, the thickness and stacking sequence of the nano laminate are optimized, and the multi-layer film structure is obtained. Finally, the manufacturing tolerance of the designed immersed grating is analyzed, and the tolerance of the grating with diffraction efficiency greater than 90% and polarization sensitivity less than 1% is presented.

**Results and Discussions** Based on the introduced design method, an immersed grating working under the total internal reflection and coated with the nano laminate is designed, and it has high diffraction efficiency and low polarization sensitivity. Benefiting from the advantages of total internal reflection, the designed immersed grating has no transmission order, and the diffraction light energy is concentrated on the reflection diffraction order, which is helpful to improve the diffraction efficiency. Additionally, the coating on the grating groove is the nano laminate structure, which is alternately stacked with Al<sub>2</sub>O<sub>3</sub> and TiO<sub>2</sub> materials (Fig. 7). The nano laminate can improve the diffraction efficiency of the grating in the transverse electricity (TE) and transverse magnetism (TM) directions, and reduce the polarization sensitivity. The results show that the average diffraction efficiency of the design immersed grating at the -1 order is higher than 92%, and the polarization sensitivity is lower than 1% in the working band of 750 – 770 nm (Fig. 8).

**Conclusions** Our paper provides the spectral resolution formula of immersed gratings based on the principle of immersed gratings and shows that the immersed grating can reduce the size of the optical system and achieve high spectral resolution. According to the working conditions and grating parameters given by the optical design, fused silica is selected as the grating substrate, and a total internal reflection immersed diffraction grating with high diffraction efficiency and low polarization sensitivity is designed. The corresponding manufacturing tolerances are analyzed by considering the diffraction efficiency and polarization sensitivity requirements and the manufacturing method. The presented reflective immersed grating in our paper has the advantages of high diffraction efficiency and low polarization, and the grating groove tolerance is feasible for manufacturing. Therefore, our study lays a basis for the design of high-performance reflective immersed gratings.

**Key words** diffraction grating; immersed grating; total internal reflection; nano laminate; diffraction efficiency; polarization sensitivity